中國機械工程學刊第四十一卷第三期第 275~287 頁(民國一百零九年)
Journal of the Chinese Society of Mechanical Engineers, Vol.41, No.3, pp 275~287 (2020)

Calculation of Tooth Surface Contact Stress and Tooth Root Bending Stress of the Asymmetric Gear with Double Pressure Angles Meshing Beyond the Pitch Point Based on Friction Between Teeth

Xiu-Lian Li*, Kam-Yim Sze**, Xu-Song Xu***, Wei Liu***, Xiao-Fang Shi***, Xian-Wei Wang*** and Hong-Tao Sun**

Keywords: asymmetric gear, contact stress, bending stress, friction between teeth, meshing beyond the pitch point.

ABSTRACT

Advantages of asymmetric gear include larger load carrying capacity, smaller vibration and longer life. The vibration of the gear system due to the change of the direction of the friction force can be avoided when meshing beyond the pitch point happens. But the meshing mechanism of asymmetric gear with double pressure angles meshing beyond the pitch point is not yet known. In this paper, the basic theory of the asymmetric gear driving system meshing beyond the pitch point is developed. Through analyzing the forces exerted on the driving gear of reducing-speed asymmetric spur gear drive system meshing beyond the pitch point in single & double pairs teeth meshing range, the contact stress and bending stress on the pinion under the action of the sliding friction between teeth— are derived. It will be seen that the contact stress and bending stress of asymmetric gear drive system meshing behind the pitch point are lower than those of the symmetric gear drive system meshing behind the pitch point, under equal conditions. And the contact stress can be effectively reduced by tuning the pressure angle of driving side, modification coefficient on pinion, the modulus and the addendum coefficient on the coast side .

Paper Received June, 2017. Revised November, 2018, Accepted April, 2019, Author for Correspondence: Xiu-Lian Li.

* *Associate Professor, The State Key Laboratory of Mechanical Transmissions, Chongqing University, 400044, Chongqing, China. School of Mechanical Engineering, Jiangsu University of Technology, Changzhou 213001, China. Zhejiang Provincial Key Laboratory of Advanced Manufacturing Technology, Hangzhou 310027, China.*

** *Department of Mechanical Engineering, The University of Hong Kong, Pokfulam, Hong Kong, China.*

*** *School of Mechanical Engineering, Jiangsu University of Technology, Changzhou 213001, China.*

INTRODUCTION

Gear drive is an important and widely used mechanical transmission device. To improve the bending strength at the gear tooth root, a new kind of asymmetric gear with double pressure angles, hereinafter referred to as asymmetric gear, was put forward. On the driving and coast sides, the pressure angles of the tooth profiles are larger and smaller, respectively. In recent years, a lot of researches on the asymmetric gear (Litvin F L et al., 2000; Deng Xiao-He et al., 2015; Li Xiu-Lian et al., 2011) have been conducted. Litvin F L, et al (2000) proposed a modified geometry of an asymmetric spur gear drive which is a combination of an involute gear and a double crowned pinion. It localizes and stabilizes the bearing contact. A favorable shape of transmission errors at reduced magnitude is obtained. Yang Shyue-Chen (2007) proposed a double envelope concept to determine the basic profile of an internal gear with asymmetric involute teeth including driving and driven gears. The advantages of asymmetric gear include larger carrying capacity, smaller volume, lighter weight and longer life.

When a gear system is driven, the friction force between the pair of gear tooth exists and changes direction before and after the pitch point. The directional change is one of the exciting factors of gear vibration, and aggravates the vibration of the gear transmission system. However, when meshing beyond the pitch point happens, i.e. the pitch point is not passed through by the meshing line of gear, the vibration of the gear system due to the change of the direction of the friction force can be avoided. According to the position of the pitch point, gears meshing beyond the pitch point can be divided into the meshing in front of the pitch point and the meshing behind the pitch point. Recently, a lot of researches (Sun Yong-Zheng et al., 2013; Ma Gang, 2000; Tian Jing-Yun et al., 2007; Liu Jing-Jing et al. , 2012) on the gear meshing beyond the pitch point have been investigated. Gao et al. (1997) proposed the feasibility of meshing beyond pitch point after a bounded optimum calculation in regard to the optimum seeking of addendum modification coefficient of gears. Li Peng et al. (2010) proposed the decision conditions and calculation method of the meshing beyond pitch point of involute gear pair with few teeth number. But all of the studies are confined to the symmetric gear drive. The meshing mechanism of asymmetric gear meshing beyond the pitch point is not yet known.

This paper considers asymmetric gear with double pressure angles in the contacting teeth. It derives the equations for the contact stress & bending stress by taking the sliding friction between teeth and the characteristic of asymmetric gear meshing beyond the pitch point into account.

MECHANISM OF ASYMMETRIC GEAR MESHING BEYOND PITCH POINT

Figure 1 shows the tooth profiles of the symmetric gear and asymmetric gear.

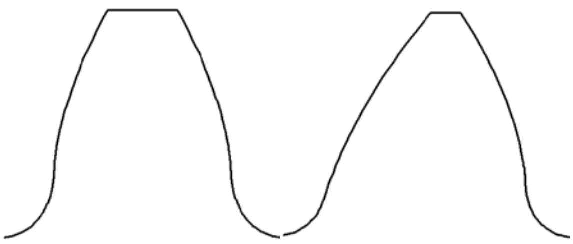

(a) (b)

Fig. 1. Tooth profile of symmetric and asymmetric gear.
(a) the tooth profile of symmetric gear
(b) the tooth profile of asymmetric gear

The involute asymmetric external gearing spur cylindrical gearing is the study object in this article. Let (z_1, z_2) be the teeth number, (m_1, m_2, m) be the moduli, (α_{d1}, α_{d2}, α_d) be the pressure angle of driving side, (α_{c1}, α_{c2}, α_c) be the pressure angle of coast side, (α_{a1d}, α_{a2d}) be the pressure angle of addendum circle of driving side, (α_{a1c}, α_{a2c}) be the pressure angle of addendum circle of coast side, α'_d be engagement angle on driving side of gear pair, α'_c be engagement angle on coast side of gear pair, (p_{bd1}, p_{bd2}) be normal direction distance between teeth on driving side, $\varepsilon_{\alpha d}$ be contact ratio on the driving side of gear pair, and $\varepsilon_{\alpha c}$ be contact ratio on the coast side of gear pair. In the afore-introduced symbols, 1 and 2 are the subscripts for the pinion and gear, respectively.

On the driving side, the distance between the two adjacent teeth of the meshing gears along the common normal line must be equal to ensure that the gear can be properly engaged. With respected to the nature of the involute gear（Li Peng 2010）, the following relations can be derived:

$$p_{bd1} = p_{bd2}, \tag{1}$$

$$p_{bd1} = \pi m_1 \cos\alpha_{d1}, \tag{2}$$

$$p_{bd2} = \pi m_2 \cos\alpha_{d2}, \tag{3}$$

Where,

$$m_1 \cos\alpha_{d1} = m_2 \cos\alpha_{d2}, \tag{4}$$

Similarly, the following relations can be derived for the coast side:

$$m_1 \cos\alpha_{c1} = m_2 \cos\alpha_{c2}, \tag{5}$$

When, $m_1=m_2=m$, $\alpha_{d1}=\alpha_{d2}=\alpha_d$, and $\alpha_{c1}=\alpha_{c2}=\alpha_c$, one has the asymmetric gear with double pressure angles driving system.

To ensure the continuity of asymmetric gear transmission, the actual meshing line should not be shorter than the base pitch. The quality of gear transmission is commonly characterized by the ratio of the actual meshing line segment and base pitch, i.e. contact ratio. The following formulas can be derived by considering the transmission characteristics of asymmetric gear:

for the driving side,

$$\varepsilon_{\alpha d} = \frac{1}{2\pi}[z_1(\tan\alpha_{a1d} - \tan\alpha'_d) + z_2(\tan\alpha_{a2d} - \tan\alpha'_d)], \tag{6}$$

for the coast side,

$$\varepsilon_{\alpha c} = \frac{1}{2\pi}[z_1(\tan\alpha_{a1c} - \tan\alpha'_c) + z_2(\tan\alpha_{a2c} - \tan\alpha'_c)], \tag{7}$$

Figure 2 shows the meshing of involute asymmetric spur cylindrical gear.

In Fig. 2, P is the pitch point; B_2 and B_1 are the start and end points on the actual meshing line, respectively; N_{1d} and N_{2d} are the tangent points of the meshing lines to the base circles of the pinion and gear, respectively; O_1 and O_2 are the centers of the pinion and gear, respectively; ω_1 and ω_2 are the angular velocities of pinion and gear, respectively. The following inequality must be fulfilled in order that the meshing occurs in front of the pitch point (see Fig. 2(b)).

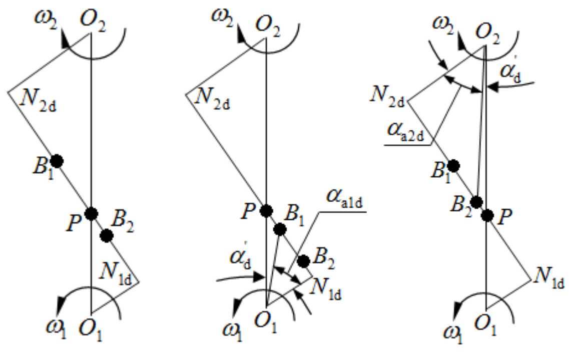

(a) (b) (c)

Fig. 2. Meshing of involute asymmetric spur cylindrical gear.
(a) Meshing on both sides of the pitch point.
(b) Meshing in front of the pitch point.
(c) Meshing behind the pitch point.

$$\overline{N_{1d}B_1} < \overline{N_{1d}P}\,, \tag{8-1}$$

or equivalently,

$$\alpha_{a1d} < \alpha_d^{'}\,, \tag{8-2}$$

For the same reason, the following inequality must be fulfilled in order that the meshing occurs behind the pitch point (see Fig. 2(c)) .

$$\overline{N_{2d}B_2} < \overline{N_{2d}P}\,, \tag{9-1}$$

or equivalently,

$$\alpha_{a2d} < \alpha_d^{'}\,, \tag{9-2}$$

The pressure angle of addendum circle on the driving side of the pinion and the gear (α_{a1d}, α_{a2d}), respectively, can be derived by considering the characteristic of asymmetric gear meshing beyond the pitch point,

$$\alpha_{a1d} = \arccos\left(\frac{r_1 \cos\alpha_d}{r_1 + h_{a1}}\right), \tag{10}$$

$$\alpha_{a2d} = \arccos\left(\frac{r_2 \cos\alpha_d}{r_2 + h_{a2}}\right), \tag{11}$$

$$h_{a1} = (h_{ac}^{*} + x_1 - \Delta y_1)m\,, \tag{12}$$

$$h_{a2} = (h_{ac}^{*} + x_2 - \Delta y_2)m\,, \tag{13}$$

$$\Delta y_1 = \left(\frac{z_2}{2} + x_2\right) + \left(\frac{z_1}{2} + x_1\right) - \frac{a}{m}\,, \tag{14}$$

$$\Delta y_2 = \left(\frac{z_1}{2} + x_1\right) + \left(\frac{z_2}{2} + x_2\right) - \frac{a}{m}\,, \tag{15}$$

$$a = \frac{(z_1 + z_2)m\cos\alpha_d}{2\cos\alpha_d^{'}}\,, \tag{16}$$

If gears are cut by rack cutters, the following inequalities must be fulfilled in order to avoid the gear meshing interference.

$$\tan\alpha_d^{'} - \frac{z_1}{z_2}(\tan\alpha_{a1d} - \tan\alpha_d^{'}) \geq \tan\alpha_d - \frac{4(h_{ac}^{*} - x_2)}{z_2\sin(2\alpha_d)}\,, \tag{17}$$

$$\tan\alpha_c^{'} - \frac{z_1}{z_2}(\tan\alpha_{a1c} - \tan\alpha_c^{'}) \geq \tan\alpha_c - \frac{4(h_{ac}^{*} - x_2)}{z_2\sin(2\alpha_c)}\,, \tag{18}$$

$$\tan\alpha_d^{'} - \frac{z_2}{z_1}(\tan\alpha_{a2d} - \tan\alpha_d^{'}) \geq \tan\alpha_d - \frac{4(h_{ac}^{*} - x_1)}{z_1\sin(2\alpha_d)}\,, \tag{19}$$

$$\tan\alpha_c^{'} - \frac{z_2}{z_1}(\tan\alpha_{a2c} - \tan\alpha_c^{'}) \geq \tan\alpha_c - \frac{4(h_{ac}^{*} - x_1)}{z_1\sin(2\alpha_c)}\,, \tag{20}$$

And, the conditions of asymmetric gear non undercut are

$$z_{1-\min} = \min\left\{\frac{2h_{ad}^{*}}{\sin^2\alpha_d}, \frac{2h_{ac}^{*}}{\sin^2\alpha_c}\right\}, \tag{21}$$

$$z_{2-\min} = \min\left\{\frac{2h_{ad}^{*}}{\sin^2\alpha_d}, \frac{2h_{ac}^{*}}{\sin^2\alpha_c}\right\}, \tag{22}$$

$$x_{1-\min} \geq \max\left\{\begin{array}{l} h_{ad}^{*} - \dfrac{z_1\sin^2\alpha_d}{2} \\ h_{ac}^{*} - \dfrac{z_1\sin^2\alpha_c}{2} \end{array}\right\}, \tag{23}$$

$$x_{2-\min} \geq \max\left\{\begin{array}{l} h_{ad}^{*} - \dfrac{z_2\sin^2\alpha_d}{2} \\ h_{ac}^{*} - \dfrac{z_2\sin^2\alpha_c}{2} \end{array}\right\}, \tag{24}$$

Further more, the following equations can be derived For avoiding addendum pointing in asymmetric gear design.

$$r_{a1} = \left(\frac{z_1}{2} + h_{ac}^{*} + x_1 - \Delta y_1\right)m\,, \tag{25}$$

$$r_{a2} = \left(\frac{z_2}{2} + h_{ac}^{*} + x_2 - \Delta y_2\right)m\,, \tag{26}$$

$$s_1 = \frac{\pi m}{2} + x_1 m(\tan\alpha_d + \tan\alpha_c)\,, \tag{27}$$

$$s_2 = \frac{\pi m}{2} + x_2 m(\tan\alpha_d + \tan\alpha_c), \tag{28}$$

$$\mathrm{inv}\alpha_d = \tan\alpha_d - \alpha_d, \tag{29}$$

$$\mathrm{inv}\alpha_c = \tan\alpha_c - \alpha_c, \tag{30}$$

$$\mathrm{inv}\alpha_{a1d} = \tan\alpha_{a1d} - \alpha_{a1d}, \tag{31}$$

$$\mathrm{inv}\alpha_{a2d} = \tan\alpha_{a2d} - \alpha_{a2d}, \tag{32}$$

$$\mathrm{inv}\alpha_{a1c} = \tan\alpha_{a1c} - \alpha_{a1c}, \tag{33}$$

$$\mathrm{inv}\alpha_{a2c} = \tan\alpha_{a2c} - \alpha_{a2c}, \tag{34}$$

$$s_{a1} = r_{a1}\left(\frac{2s}{mz_1} + \mathrm{inv}\alpha_d + \mathrm{inv}\,\alpha_c - \mathrm{inv}\,\alpha_{a1d} - \mathrm{inv}\,\alpha_{a1c}\right), \tag{35}$$

$$s_{a2} = r_{a2}\left(\frac{2s}{mz_2} + \mathrm{inv}\alpha_d + \mathrm{inv}\,\alpha_c - \mathrm{inv}\,\alpha_{a2d} - \mathrm{inv}\,\alpha_{a2c}\right), \tag{36}$$

where, (r_1, r_2) are the reference circle radii, (r_{a1}, r_{a2}) are the addendum circle radii, (h_{a1}, h_{a2}) are the addendums, (x_1, x_2) are the modification coefficients, (Δy_1, Δy_2) are the coefficients of variation on addendum, (h^*_{ac}, h^*_{ad}) are the addendum coefficients on the driving side and coast side, respectively. a is the actual center distance between the pinion and the gear, (s_1, s_2) are the tooth thicknesses of reference circle, (s_{a1}, s_{a2}) are the tooth thicknesses of addendum circle, (invα_d, invα_c, invα_{a1d}, invα_{a2d}, invα_{a1c}, invα_{a2c}) are the involute functions of α_d, α_c, α_{a1d}, α_{a2d}, α_{a1c}, and α_{a2c}, respectively. In the afore- introduced symbols, 1 and 2 are the subscripts for the pinion and the gear, respectively.

ANALYSIS OF ENGAGING FORCE IN ASYMMETRIC GEAR

Figure 3 shows the engaging force F_n and friction force F_μ acting on the driving side of the asymmetric gears, within the single pair teeth meshing range.

When random engaging point M is in single pair teeth meshing area (see Figure 4 and 5) , dynamic force balance yields

$$F_n r_{bd1} + F_\mu \lambda L_1 = T_1, \tag{37}$$

and

$$F_\mu = \mu F_n, \tag{38}$$

where, T_1 is the driving torque of the pinion, r_{bd1} is the base circle radius on driving side of the pinion, λ is direction coefficient of friction force, L_1 is the moment arm of F_μ with respect to O_1, and μ is coefficient of sliding friction between teeth surfaces. From Equation (37) and (38),

$$F_n = \frac{T_1}{\mu L_1 \lambda + r_{bd1}}, \tag{39}$$

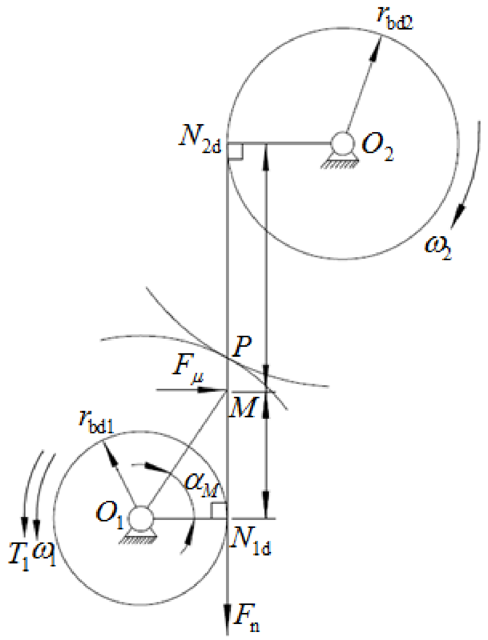

Fig. 3. Model of mechanics of the asymmetric gears

Similar derivation applies when the random engaging point M is in double pairs teeth meshing area. It can be deduced from Figure 4 and 5 which show the meshing lines beyond pitch point that

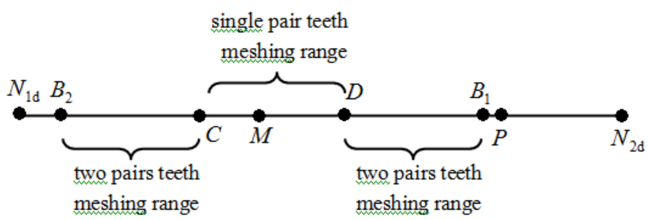

Fig. 4. Meshing line in front of the pitch point

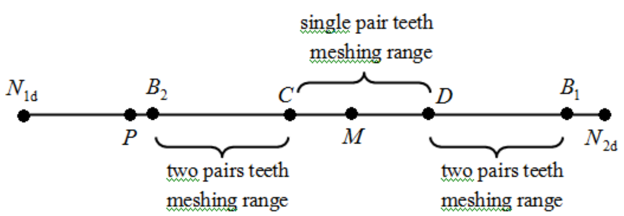

Fig. 5. Meshing line behind the pitch point

$$F_n r_{bd1} + F_{\mu 1}\lambda L_1 + F_{\mu 2}\lambda(L_1 + p_{bd1}) = T_1, \tag{40}$$

Suppose the engaging force in double pairs teeth meshing area is divided equally, i.e.

$$F_{\mu 1} = F_{\mu 2} = \mu F_n / 2, \tag{41}$$

From the last two equations,

$$F_{\mathrm{n}} = \frac{2T_1}{2\mu L_1\lambda + 2r_{\mathrm{bd1}} + \mu\lambda p_{\mathrm{bd1}}}, \tag{42}$$

Other parameters by considering the characteristic of asymmetric gear meshing beyond the pitch point are given as

$$\lambda = \mathrm{sign}(\omega_1 L_1 - \omega_2 L_2) = \begin{cases} 1 & (\omega_1 L_1 > \omega_2 L_2) \\ 0 & (\omega_1 L_1 = \omega_2 L_2) \\ -1 & (\omega_1 L_1 < \omega_2 L_2) \end{cases}, \tag{43}$$

$$L_1 = r_{\mathrm{bd1}} \tan\alpha_{\mathrm{M}}, \tag{44}$$

$$L_2 = (r_{\mathrm{bd1}} + r_{\mathrm{bd2}})\tan\alpha'_{\mathrm{d}} - r_{\mathrm{bd1}}\tan\alpha_{\mathrm{M}}, \tag{45}$$

$$\theta_{\alpha'_{\mathrm{d}}} = \frac{2(x_2 + x_1)\tan\alpha_{\mathrm{d}} + (z_2 + z_1)\mathrm{inv}\alpha_{\mathrm{d}}}{z_1 + z_2}, \tag{46}$$

$$A = \sin\{\arctan[(3\theta_{\alpha'_{\mathrm{d}}})^{\frac{1}{3}} + \frac{3\theta_{\alpha'_{\mathrm{d}}}}{5} + \frac{\theta^{1.6}_{\alpha'_{\mathrm{d}}}}{11}]\}, \tag{47}$$

$$Q = \theta_{\alpha'_{\mathrm{d}}} + \arctan[(3\theta_{\alpha'_{\mathrm{d}}})^{\frac{1}{3}} + \frac{3\theta_{\alpha'_{\mathrm{d}}}}{5} + \frac{\theta^{1.6}_{\alpha'_{\mathrm{d}}}}{11}], \tag{48}$$

$$\alpha'_{\mathrm{d}} = \arccos\left\{\frac{A}{Q}\right\}, \tag{49}$$

where, L_2 is the moment arm of friction force on point O_2, α_{M} is the pressure angle of random meshing point M ; $\theta_{\alpha'\mathrm{d}}$ are the involute functions on the driving side of the gear pair.

CALCULATION OF CONTACT STRESS OF ASYMMETRIC GEAR

From Hertz theory (Pu Liang-Gui et al. , 2013), the contact normal stress on the tooth surface of the asymmetrical involute gear is

$$\sigma_{\mathrm{y}} = \sqrt{\frac{E_\Sigma F_{\mathrm{n}}}{\pi R_\Sigma b}}, \tag{50}$$

In the expression, b is face width whilst the equivalent elastic modulus E_Σ of the contact pair and the comprehensive radius of curvature R_Σ of the engaging point are

$$\frac{1}{E_\Sigma} = \frac{1-\nu_1^2}{E_1} + \frac{1-\nu_2^2}{E_2}, \tag{51}$$

$$\frac{1}{R_\Sigma} = \frac{1}{R_{(\mathrm{M})1}} + \frac{1}{R_{(\mathrm{M})2}}, \tag{52}$$

where E is elastic modulus, v is Poisson's ratio, $R_{(\mathrm{M})}$ is the radius of curvature of the random engaging point M, “1” is the subscript for pinion and “2” is the subscript for the gear. Moreover,

$$R_{(\mathrm{M})1} = \overline{N_{1\mathrm{d}}M} = L_1, \tag{53}$$

$$R_{(\mathrm{M})2} = \overline{N_{2\mathrm{d}}M} = L_2, \tag{54}$$

The infinitesimal volume shown in Figure 6 is cut out from the meshing point M of the pinion to illustrate the stress components acting.

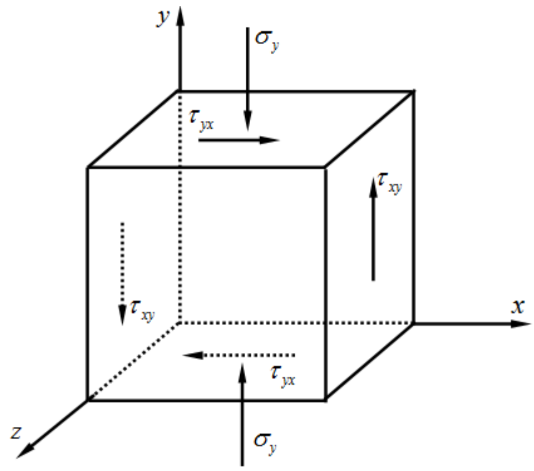

Fig. 6. The stress acting on an infinitesimal volume

With $\tau_{xy}=\tau_{yx}=\mu\sigma_y$, and other stress components being zero, the von Mises stresses is

$$\sigma_{\mathrm{H}} = \sqrt{\sigma_y^2 + 3\tau_{xy}^2} = \sigma_y\sqrt{1+3\mu^2} \approx \sigma_y(1+\frac{3}{2}\mu^2), \tag{55}$$

As μ seldom exceeds 0.2 in gear systems, the above stress is dominated by the normal stress σ_y. By incorporating the σ_y, in Eqn. (55),

$$\sigma_{\mathrm{H}} = \sqrt{\frac{(1+3\mu^2)E_\Sigma F_{\mathrm{n}}}{\pi R_\Sigma b}}, \tag{56}$$

which is often taken to the contact stress under the combined action of the normal contact stress and the shear friction stress.

CALCULATION OF BENDING STRESS OF ASYMMETRIC GEAR

Taking the center O_1 of the base circle of the pinion as the origin of coordinate and the axis y is drawn from O_1 to L which is the intersection of the driving side and the coast side. The rectangular coordinate system as shown in Figure 7 is established.

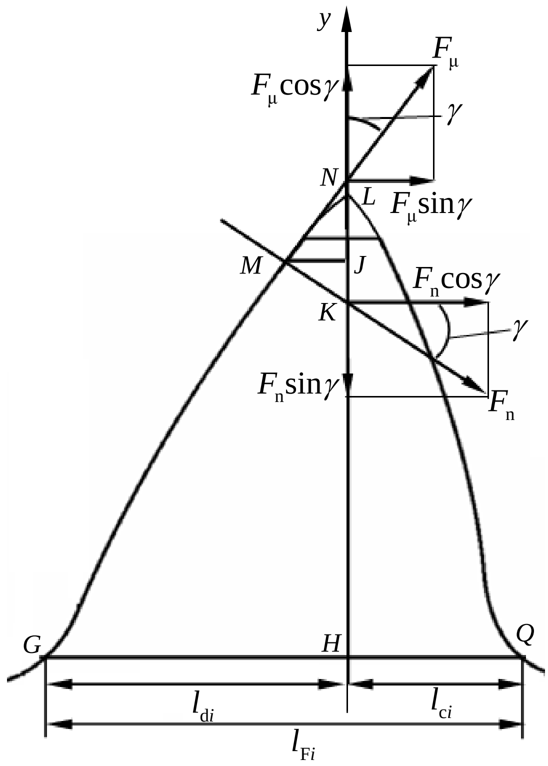

Fig. 7. Force model of the pinion tooth

Compared with the symmetrical involute cylindrical gear, the dangerous section of tooth root of asymmetrical involute cylindrical gear can not be determined by 30 degree tangent method. The bending stress of asymmetrical gear with double pressure angles tooth root is calculated by plain section method, i.e., a series of planes perpendicular to the axis y are drawn through the gear's transition curve, then the corresponding sections of gear are obtained, and the section corresponding to the maximum bending stress on tooth root is the dangerous section.

Fig. 7 shows the engaging force F_n and friction force F_μ acting on the driving side of the asymmetric gears, corresponding to random engaging point M. F_n is moved from point M to point K on the axis y along the meshing line, and F_μ is moved from point M to point N on the axis y along the tangent line of involute, in order for easy analyses. G and Q, are the random point of the tooth root transition curve on drive side or coast side, respectively. Only the bending stress is considered for simplified calculation. So the primitive value of bending stress on the tooth root of the asymmetrical involute gear is

$$\sigma_F = \frac{6F_n h_{Fi}[1+f(1+\frac{\Delta h_i}{h_{Fi}})\tan\gamma]\cos\gamma}{bl_{Fi}^2}, \tag{57}$$

After the introductions of tooth profile coefficient Y_{Fai} and stress correction factor Y_{Sai} ,

$$\sigma_F = Y_{Fai}Y_{Sai}\frac{F_n\cos\alpha_d}{bm}\cdot [1+f(1+\frac{\Delta h_i}{h_{Fi}})\tan\gamma], \tag{58}$$

and

$$Y_{Fai} = \frac{6(h_{Fi}/m)\cos\gamma}{(l_{Fi}/m)^2\cos\alpha_d}, \tag{59}$$

$$Y_{Sai} = \frac{1.2h_{Fi}+0.13l_{Fi}}{h_{Fi}}\left(\frac{l_{Fi}}{2\rho_{Fi}}\right)^{\frac{l_{Fi}}{1.21l_{Fi}+2.3h_{Fi}}}, \tag{60}$$

where, γ named load angle, is the sharp angle between the tangent line of the involute passing through point M and the axis y, h_{Fi} is the distance from point K to line GQ of risk section, Δh_i is the distance from point K to point N, ρ_{Fi} is the curvature radius of the intersection point between the dangerous section and the drive side. l_{Fi} , l_{di} and l_{ci} are the lengths of random plain section, the drive side, and the coast side, on the tooth root, respectively.

The bending stress of tooth root of asymmetric gear meshing beyond the pitch point is calculated on the tooth top, i.e. point B_1, and processed on the basis of the single pair teeth meshing, for easy analyses.

The values of Δh_i and F_n are (Xu Fu-Ren, Shen Wei, 2001)

$$\Delta h_i = \overline{MJ}(\tan\gamma+\cot\gamma) \approx \delta_{MJ}(\tan\gamma+\cot\gamma), \tag{61}$$

$$\delta_{MJ} = \frac{\pi r_M}{2z_1} - r_M(\mathrm{inv}\alpha_M - \mathrm{inv}\alpha_{d1}), \tag{62}$$

where, δ_{MJ} is the circular tooth thickness of arc MJ, r_M is the distance between point M to point O_1.

The coordinates of point G (x, y) and Q (x, y) are (Xiao Wang-Qiang et al. 2008), respectively

$$x_G = -\frac{mz_1}{2}\sin\phi_d + (r_\rho + \frac{\delta a - x_1 m}{\sin\alpha_{gd}})\cdot \cos(\alpha_{gd}-\phi_d), \tag{63}$$

$$y_G = \frac{mz_1}{2}\cos\phi_d - (r_\rho + \frac{\delta a - x_1 m}{\sin\alpha_{gd}})\cdot \sin(\alpha_{gd}-\phi_d), \tag{64}$$

$$\phi_{\mathrm{d}} = \frac{2[(\delta a - x_1 m)\cot\alpha_{\mathrm{gd}} + \dfrac{\pi m}{2}]}{m z_1}, \quad \alpha_{\mathrm{gd}} \in (\alpha_{\mathrm{d}}, 90°) \tag{65}$$

$$x_Q = -\frac{m z_1}{2}\sin\phi_{\mathrm{c}} - (r_\rho + \frac{\delta a - x_1 m}{\sin\alpha_{\mathrm{fc}}})\cdot \cos(\alpha_{\mathrm{fc}} - \phi_{\mathrm{c}}), \tag{66}$$

$$y_Q = \frac{m z_1}{2}\cos\phi_{\mathrm{c}} - (r_\rho + \frac{\delta a - x_1 m}{\sin\alpha_{\mathrm{fc}}})\cdot \sin(\alpha_{\mathrm{fc}} - \phi_{\mathrm{c}}), \tag{67}$$

$$\phi_{\mathrm{c}} = \frac{2[(\delta a - x_1 m)\cot\alpha_{\mathrm{fc}} + \dfrac{\pi m}{2}]}{m z_1}, \quad \alpha_{\mathrm{fc}} \in (\alpha_{\mathrm{c}}, 90°) \tag{68}$$

The length of random plain section $l_{\mathrm{F}i}$ is

$$l_{\mathrm{F}i} = l_{\mathrm{d}i} + l_{\mathrm{c}i} = |x_{Gi}| + x_{Qi}, \tag{69}$$

where, x_{Gi} and x_{Qi} are the horizontal coordinates of intersection point between random plain section and the tooth root transition curve, on driving side or coast side, respectively. α_{gd} and φ_{d}, α_{fc} and φ_{c}, are all transition parameters.

From Euler—Savary formula, the curvature radius $\rho_{\mathrm{F}i}$ is (Xiao Wang-Qiang 2008)

$$\rho_{\mathrm{F}i} = \frac{\delta a - x_1 m}{\sin\alpha_{\mathrm{gd}}} + r_\rho - \frac{m z_1(\delta a - x_1 m)\sin\alpha_{\mathrm{gd}}}{2(\delta a - x_1 m) + m z_1(\sin\alpha_{\mathrm{gd}})^2}, \tag{70}$$

By considering the characteristic of asymmetric gear, $h_{\mathrm{F}i}$ is given as

$$h_{\mathrm{F}i} = \frac{m z_1\cos\alpha_{\mathrm{d}}}{2\cos\gamma} - \frac{m z_1}{2}\cos\phi_{\mathrm{d}} + (\frac{\delta a - x_1 m}{\sin\alpha_{\mathrm{gd}}} + r_\rho)\sin(\alpha_{\mathrm{gd}} - \phi_{\mathrm{d}}), \tag{71}$$

When meshing at the point B_1,

$$\gamma = \gamma_{B_1} = \tan\alpha_{B_1} - \mathrm{inv}\alpha_{\Delta d}. \tag{72}$$

Where, r_ρ is the fillet radius of the gear hob top, δa is the distance from the center of r_ρ to midline of rack, $\alpha_{\Delta\mathrm{d}}$ is the pressure angle of L on driving side.

RESULTS & DISCUSSIONS

The above analysis shows that the contact stress and bending stress of asymmetric gear meshing beyond the pitch point varies with the pressure angle, friction coefficient, addendum modification coefficient, etc.

Figure 8 shows how the contact stress of gear changes with the engagement line. The gear parameters used in the analysis of the four cases are listed in Table 1.

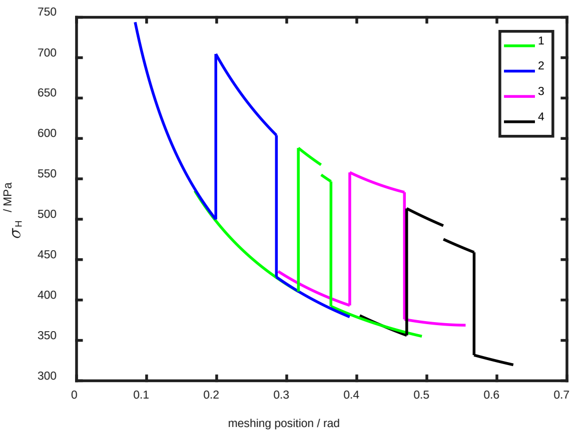

Fig. 8. Distribution of contact stress

Case 1: symmetric gear driving meshing on both sides of the pitch point
Case 2: symmetric gear driving meshing in front of the pitch point
Case 3: symmetric gear driving meshing behind the pitch point
Case 4: asymmetric gear driving meshing on both sides of the pitch point

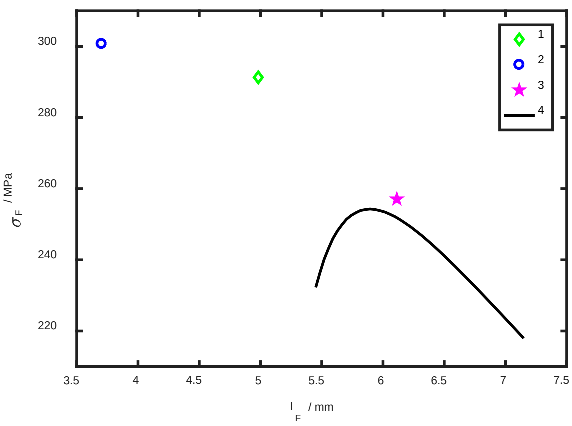

Fig. 9. Distribution of bending stress

From Fig. 8 and 9, the contact stress and bending stress of asymmetric gear drive are the lowest, the contact stress and bending stress of symmetric gear drive meshing behind the pitch point are lower than those of meshing on both sides of pitch point, whilst the contact stress and bending stress of symmetric gear drive meshing in front of the pitch point are the highest. The maximum contact stresses are 557.9 and 513.3MPa in cases 3 and 4 in Fig. 8, respectively. Thus, the tooth surface contact stress will be reduced by 8.0% in the asymmetric gear drive mechanism .

Figure 10 and 11 show the contact stress and bending stress of asymmetric gear changes with the engagement line.

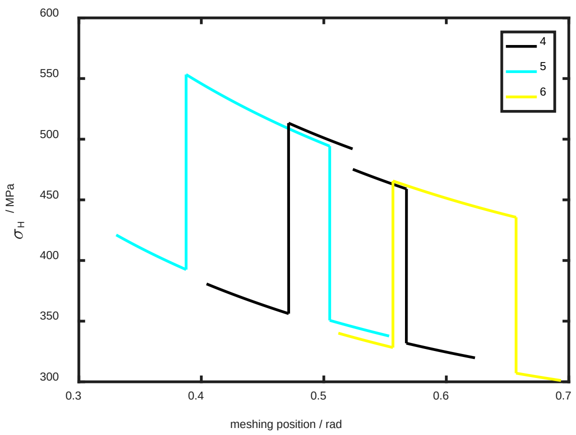

Fig. 10. Distribution of contact stress of asymmetric gear

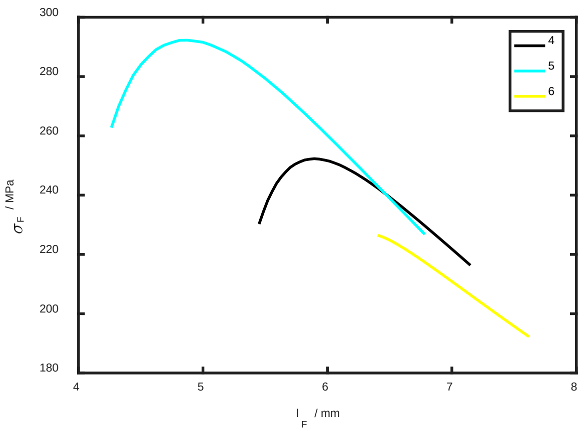

Fig. 11. Distribution of bending stress of asymmetric gear

The gears in case 4 is meshing on both sides of the pitch point, the gears in case 5 is meshing in front of the pitch point, the gears in case 6 is meshing behind the pitch point. The pressure angle on the driving side α_d is 30°, and the pressure angle on the coast side α_c is 20° in the three cases. In case 5, x_1 = -0.7, x_2 = 1.9. In case 6, x_1 = 0.9, x_2 = -1.4. Other parameters not mentioned are given in Table 1.

From Fig. 10 and 11, the contact stress and bending stress of asymmetric gear drive meshing behind pitch point are the lowest, whilst the contact stress and bending stress of asymmetric gears meshing in front of the pitch point are the highest. The maximum values of contact stresses and bending stress are 513.3, 252.29, 465.6, and 226.46MPa in cases 4 and 6, respectively. Thus, the tooth surface contact stress and tooth root bending stress in asymmetric gear drive mechanism meshing behind the pitch point is 9.29% and 10.24% lower than meshing on both sides of the pitch point, respectively.

It can be also seen from Fig. 8 to 11 that the contact stress and bending stress is 16.5% and 11.9% lower in asymmetric gear drive mechanism meshing behind the pitch point than in symmetric gear drive mechanism meshing behind the pitch point.

Figure 12 shows the contact stress of asymmetric gear meshing behind the pitch point changes with the pressure angles of driving side.

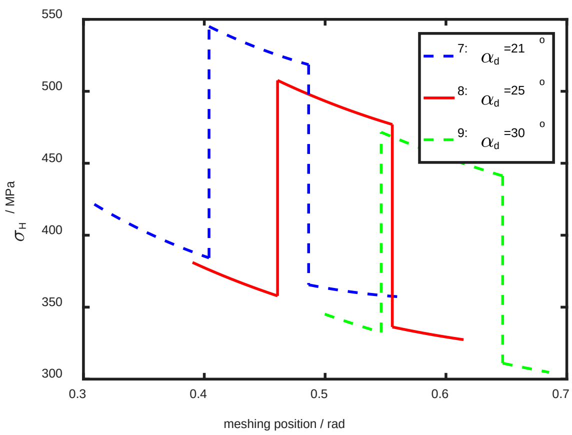

Fig. 12. Contact stress of asymmetric gear changing with the driving side pressure angles

The gear parameters used in the analysis are given. In cases 7 and 8, x_1, x_2 and α_d is 0.7, -1.9, 21° and 25°, respectively. In case 9, x_1 is 0.8, x_2 is -1.7, and α_d is 30° .Other parameters are the same as those in Table 1.

It can be seen from Fig. 12 that the contact stress of asymmetric gear drive meshing behind the pitch point is getting smaller and smaller with the increase of pressure angle on driving side. The maximum contact stress are 545.1 and 471.6MPa in cases 7 and 9, respectively. Thus, tooth surface contact stress will be reduced by 13.5% with the increase of pressure angle on driving side in asymmetric gear drive mechanism meshing behind the pitch point.

Figure 13 shows the contact stress of asymmetric gear meshing behind the pitch point changes with the engagement line based on the different friction coefficients.

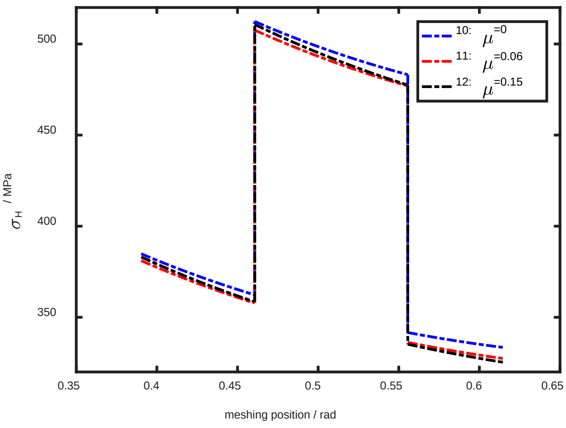

Fig. 13. Contact stress of asymmetric gear changing with the friction coefficient between teeth

In the three considered cases, μ is taken to be 0, 0.06 and 0.15 in cases 10, 11 and 12, respectively. And α_d, α_c, m, x_1, and x_2 are the same as those in case 8. When μ is 0 and 0.15, the maximum contact stresses are 512.35 and 510.7MPa, respectively. Thus, the influence of the friction between teeth on contact stress of asymmetric gear meshing behind the pitch point will be omitted.

Figure 14(a) and (b) shows the contact stress of asymmetric gear meshing behind the pitch point changes with the modification coefficient on the pinion, and the gear, respectively.

In cases 13 and 14, x_1 is 0.8 and 0.9, respectively. Other parameters used are the same as those in case 8. In cases 15, and 16, x_2 is -1.7, and -1.8, respectively. Unspecified parameters are the same as those of case 8. Other parameters not mentioned in case 8 are given in Table 1.

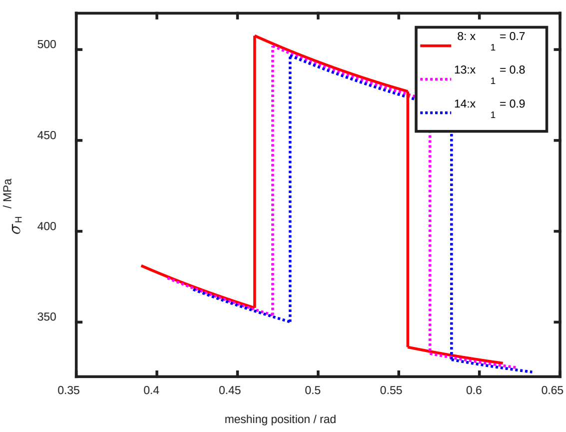

(a)

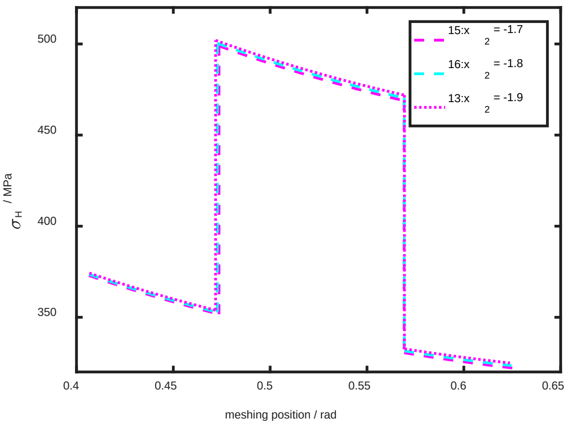

(b)

Fig. 14. Contact stress changing with the modification coefficient

From Fig. 14(a), the contact stress diminishes with the increase of modification coefficient on the pinion. The maximum contact stress are 507.6 and 469.7MPa in cases 8 and 14, respectively. Thus, the contact stress will be reduced by 7.5% with the increase of modification coefficient. But Fig. 14(b) shows that the influence of modification coefficient on the gear on contact stress can be neglected under certain conditions.

Figure 15 shows the contact stress of asymmetric gear meshing behind the pitch point changes with the moduli.

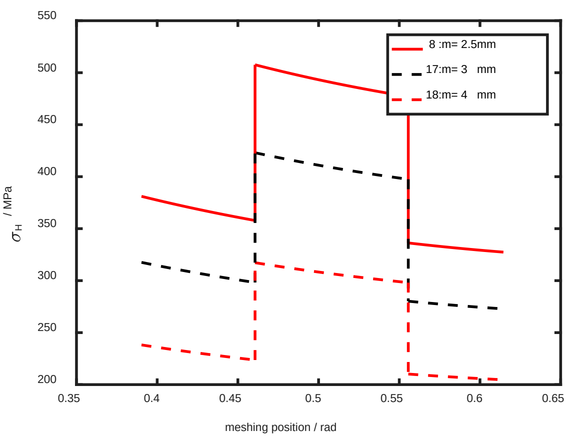

Fig. 15 Contact stress changing with the moduli

Cases 17, and 18 in Fig. 15 are obtained by changing m in case 8 to 3, and 4mm, respectively. Unspecified parameters are given in Table 1. From Fig. 15, the contact stress of asymmetric gear meshing behind the pitch point diminishes will decrease with the increase of moduli. The maximum contact stress are 507.61 and 317.26MPa in cases 8 and 18, respectively. Thus, the contact stress will be reduced by 37.5% with the increase of moduli.

Fig. 16 shows the contact stress of asymmetric gear meshing behind the pitch point changes with the addendum coefficient on the coast side.

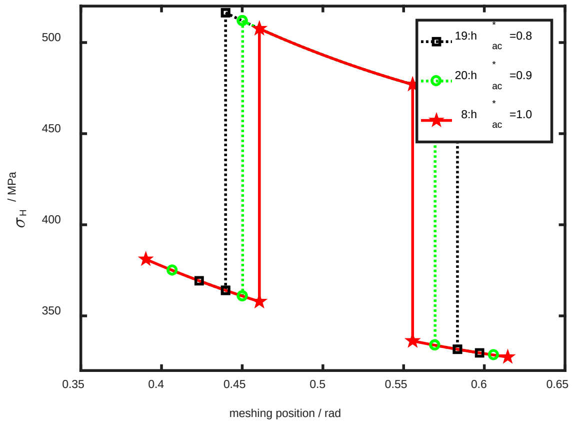

Fig. 16. Contact stress changing with the addendum coefficient on the coast side

In cases 19, 20, h_{ac}^{*} are 0.8 and 0.9, respectively. Other parameters not mentioned are the same as that in case 8. The maximum tooth surface contact stress are 516.37 and 507.61MPa when h_{ac}^{*} is 0.8, and 1.0, respectively. Thus, the maximum tooth surface contact stress will change slightly with the increase of addendum coefficient on the coast side.

Table 1: Data of Sample Gear Pairs.

	Case 1	Case 2	Case 3	Case 4	Case 5	Case 6	Case 7	Case 8	Case 9	Case 10	Case 11
z_1	30	30	30	30	30	30	30	30	30	30	30
z_2	96	96	96	96	96	96	96	96	96	96	96
m / mm	2.5	2.5	2.5	2.5	2.5	2.5	2.5	2.5	2.5	2.5	2.5
α_d / °	20	20	20	30	30	30	21	25	30	25	25
α_c / °	20	20	20	20	20	20	20	20	20	20	20
b / mm	75	75	75	75	75	75	75	75	75	75	75
h_{ac}^{*}	1	1	1	1	1	1	1	1	1	1	1
μ	0.12	0.12	0.12	0.12	0.12	0.12	0.12	0.12	0.12	0	0.06
x_1	0	-0.7	0.7	0	-0.7	0.9	0.7	0.7	0.8	0.7	0.7
x_2	0	1.8	-1.9	0	1.9	-1.4	-1.9	-1.9	-1.7	-1.9	-1.9
E / GPa	206	206	206	206	206	206	206	206	206	206	206
v	0.25	0.25	0.25	0.25	0.25	0.25	0.25	0.25	0.25	0.25	0.25
n_1 / rpm	1440	1440	1440	1440	1440	1440	1440	1440	1440	1440	1440
T_1 / N·m	230	230	230	230	230	230	230	230	230	230	230

Continued table 1

	Case 12	Case 13	Case 14	Case 15	Case 16	Case 17	Case 18	Case 19	Case 20
z_1	30	30	30	30	30	30	30	30	30
z_2	96	96	96	96	96	96	96	96	96
m / mm	2.5	2.5	2.5	2.5	2.5	3	4	2.5	2.5
α_d / °	25	25	25	25	25	25	25	25	25
α_c / °	20	20	20	20	20	20	20	20	20
b / mm	75	75	75	75	75	75	75	75	75
h^*_{ac}	1	1	1	1	1	1	1	0.8	0.9
μ	0.15	0.12	0.12	0.12	0.12	0.12	0.12	0.12	0.12
x_1	0.7	0.8	0.9	0.7	0.7	0.7	0.7	0.7	0.7
x_2	-1.9	-1.9	-1.9	-1.7	-1.8	-1.9	-1.9	-1.9	-1.9
E / GPa	206	206	206	206	206	206	206	206	206
ν	0.25	0.25	0.25	0.25	0.25	0.25	0.25	0.25	0.25
n_1 / rpm	1440	1440	1440	1440	1440	1440	1440	1440	1440
T_1 / N·m	230	230	230	230	230	230	230	230	230

CONCLUSIONS

The basic theory of the asymmetric gear with double pressure angles driving system meshing beyond the pitch point has been developed for the first time. The mathematical models of the stress on the tooth surface and on the tooth root of the pinion is set up, under the action of friction between teeth, through analyzing the forces exerted on the pinion of reducing speed asymmetric spur gear drive system with double pressure angles in the single & double pair teeth meshing range. The calculation formulas of tooth surface contact stress and tooth root bending stress on the pinion meshing beyond the pitch point is derived. The following conclusions can be drawn from this research after conducting a large number of cases studies:

(1) For the symmetric and asymmetric gears, the contact stress and bending stress meshing behind the pitch point are lower than those of meshing on both sides of pitch point, and the contact stress and bending stress meshing in front of the pitch point are larger than those of meshing on both sides of pitch point.

(2) The contact stress and bending stress of asymmetric gear drive system meshing behind the pitch point are lower than those of the symmetric gear drive system meshing behind the pitch point, under equal conditions.

(3) The influence of friction between teeth on the contact stress of asymmetric gear drive system can be neglected when meshing behind the pitch point.

(4) Improvements in the pressure angle of driving side, modification coefficient on the pinion, the modulus, and the addendum coefficient on the coast side, are effective measures to reduce the contact stress of asymmetric gear drive meshing behind the pitch point.

CONFLICT OF INTEREST

None declared.

ACKNOWLEDGMENTS

This project is supported by National Natural Science Foundation of China (Grant No. 51475219), the State Key Laboratory of Mechanical Transmissions (SKLMT-KFKT-201614), Jiangsu Overseas Research & Training Program for University Prominent Young & Middle-aged Teachers and Presidents, Zhejiang Provincial Key Laboratory of Advanced Manufacturing Technology, and Changzhou Key Laboratory of Equipment Remanufacture Engineering (CRM2018B0 1). Part of the work was completed when the first author was visiting the University of Hong Kong in the Program.

REFERENCES

Cavdar Kadir, Karpat Fatih, Babalik Fatih C.. "Computer aided analysis of bending strength of involute spur gears with asymmetric profile", *Journal of Mechanical Design*, vol. 127, pp. 477-484 (2005).

Deng Gang, Nakanishi T., Inoue K.. "Bending load capacity enhancement using an asymmetric tooth profile (1st report, influences of pressure angle on tooth root stress and bending stiffness)", *JSME International Journal, series C*, vol. 46, No. 3, pp. 1171-1177 (2003).

Deng Xiao-He, Hua Lin, Han Xing-Hui. "Research on the design and modification of asymmetric spur gear", *Mathematical Problems in Engineering*, Article ID 897257, pp. 1-13 (2015).

Dhorje M., Ekwaro-Osire S., Khandarker M. P. H., et al. "A weibull failure theory for contact loading in gears with asymmetric teeth", *Proceedings of ASME 2008 International Mechanical Engineering Congress and Exposition*. Boston, Massachusetts, USA, pp. 1-6 (2008).

Gao Ming, Zhou Ying. "Optimization of spur cylindrical modification coefficient gear with meshing beyond pitch point", *Machinery*, Vol. 24, pp. 2-4 (1997).

Karpat Fatih, Ekwaro-Osire S.. "Wear of involute spur gears with asymmetric teeth under dynamic loading", *Proceedings of ASME 2006 International Mechanical Engineering Congress and Exposition*. Chicago, Illinois, USA, pp. 1-9 (2006).

Karpat Fatih, Ekwaro-Osire S., Cavdar Kadir, et al. "Dynamic analysis of involute spur gears with asymmetric teeth", *International Journal of Mechanical Sciences*, vol. 50, pp. 1598-1610 (200 8).

Li Peng, Wang Bao-Min, Zhang Guo-Hao. "Study on the meshing beyond pitch point of involute gear pair with few teeth number", *Mechanical Engineer*, Vol. 10, pp. 15-17 (2010).

Li Wei, Liu Yan-Jun, Qiu Li-Fang, et al, "Theory and method of hob design for a new-style asymmetric gear", *Journal of University of Science and Technology Beijing*, vol. 29, pp. 837-840. (2007)

Li Xiu-Lian, Wang Gui-Cheng, Zhu Fu-Xian, et al. "Calculation of bending stress of the asymmetric gear tooth root based on friction between teeth", *Acta Armamentarii*, vol. 32, No. 7, pp. 884-889 (2011).

Li Xiu-Lian，Wang Gui-Cheng，Zhu Fu-Xian, et al. "Calculation based on interteeth friction on contact fatigue strength of asymmetric gear", *Journal of Nanjing University of Science and Technology* (*Natral Science*), Vol. 35, pp. 76-79. (2011).

Litvin F. L., Lian Qi-Ming, Kapelevich A. L.. "Asymmetric modified spur gear drives: reduction of noise, localization of contact, simulation of meshing and stress analysis", *Comput. Methods Appl. Mech. Engrg*., vol. 188, pp. 363-390 (2000).

Liu Jing-Jing, Zhu Ru-Peng, Bao He-Yun. "Analysis of contact stress of node external gear Pair", *Machine Building & Automation*, Vol. 41, pp. 28-30 (2012).

Ma Gang. "Performance analysis of gear drive with equivocal modification meshing beyond pitch point", *Journal of Jiangsu radio ＆television university*, Vol. 11, pp. 23-24(2000).

Pedersen Niels L.. "Improving bending stress in spur gears using asymmetric gears and shape optimization". *Mechanism and Machine Theory*, vol. 45, pp. 1707-1717 (2010).

Pu Liang-Gui, Chen Guo-Ding, Wu Li-Yan, *Machine Design*. Higher Education Press, Beijing, (2013).

Sekar R. Prabhu, Muthuveerappan G. "Load sharing based maximum fillet stress analysis of asymmetric helical gears designed through direct design — A parametric study", *Mechanism and Machine Theory*, vol. 80, pp. 84-102 (2014).

Sun Yong-Zheng, Zhu Ru-Peng, Bao He-Yun. "Calculation of mean friction coefficient in scuffing strength for gear drive with meshing beyond pitch point", *Journal of Aerospace Powe*r, Vol. 28, pp. 2155-2160 (2013).

Tian Jing-Yun, Wang Bao-Min, Zhang Guo-Hai. "Study of involutes cylindrical gear pair's emerging node external gearing", *Journal of Shanxi University of Technology*, Vol. 23, pp. 5-7(2007).

Xiao Wang-Qiang. "Investigation on meshing theory and load capacity of high performance unsymmetric gear with double pressure angles". Beijing, University of Science and Technology Beijing (2008).

Xiao Wang-Qiang, Li Wei, Han Jian-You, et al. "Theoretical analysis and experiment for asymmetric gear on bending fatigue strength". *Chinese Journal of Mechanical Engineering*, Vol. 44, pp. 44-50 (2008).

Xu Fu-Ren, Shen Wei. "Effect of friction between teeth on the bending fatigue stress at the root of gear tooth". Acta Armamentarii, Vol. 22, pp. 520-524 (2001).

Yang Shyue-Cheng. "Study on an internal gear with asymmetric involute teeth". *Mechanism and Machine Theory*, vol. 42, pp. 977-994 (2007).

NOMENCLATURE

z_1 teeth number in pinion
z_2 teeth number in gear
m module
α_d pressure angle on driving side
α_c pressure angle on coast side
b face width
h_{ac}^* addendum coefficient on coast side
μ friction coefficient
x_1 addendum modification coefficient in pinion
x_2 addendum modification coefficient in gear
E Elasticity modulus
v Poisson's ratio
n_1 pinion speed
T_1 driving torque

基於齒面摩擦的雙壓力角非對稱齒輪節點外嚙合齒面接觸應力和齒根彎曲應力的計算

李秀蓮
重慶大學機械傳動國家重點實驗室
江蘇理工學院機械工程學院
浙江省先進製造技術重點實驗室

佘錦炎
香港大學機械系

徐旭松 劉偉 施曉芳 汪獻偉
江蘇理工學院機械工程學院

孫洪濤
香港大學機械系

摘要

雙壓力角非對稱齒輪具有承載能力大、振動小、壽命長等優點。一系列的研究表明，對稱齒輪節點外嚙合可避免由於摩擦力方向的改變所引起的齒輪傳動系統的振動。截至目前，雙壓力角非對稱齒輪節點外嚙合傳動的工作機理尚未可知。本文首先給出了雙壓力角非對稱齒輪節點外嚙合傳動的基本原理。然後以一對雙壓力角非對稱減速直齒圓柱齒輪節點外嚙合傳動系統為研究物件，在建立輪齒受力模型的基礎上，通過對單、雙齒嚙合區域進行受力分析，推導出齒面摩擦下，主動小齒輪的齒面接觸應力和齒根彎曲應力的計算公式。研究發現，同等條件下，雙壓力角非對稱齒輪節點後嚙合的齒面接觸應力和齒根彎曲應力均小於對稱齒輪的。進一步的研究還表明，為了有效地降低齒面接觸應力，可採取調整工作側壓力角、小齒輪的變位係數、模數和非工作側齒頂高係數等措施。